Transmembrane epitope delivery by passive protein threading through the pores of the OmpF porin trimer

Sejeong Lee[1], Nicholas G. Housden[2], Sandra A. Ionescu[1], Matthew H. Zimmer[1,3], Renata Kaminska[2], Colin Kleanthous[2], Hagan Bayley[1]*

[1]Chemistry Research Laboratory, University of Oxford, Oxford, OX1 3TA, UK

[2]Department of Biochemistry, University of Oxford, Oxford, OX1 3QU, UK

[3]current address: Arthur Amos Noyes Laboratory of Chemical Physics, California Institute of Technology, Pasadena, CA 91125, US

*Corresponding author: Hagan Bayley

Email: hagan.bayley@chem.ox.ac.uk

Supplementary Information

Table of Contents

Figure S1. Pre-equilibrium fluorescence measurements for the OmpF–OBS1 complex formation and dissociation at different salt concentrations and pH values.
Figure S2. Concentration dependence of OBS12-18 peptide binding to the periplasmic side of OmpF.
Figure S3. Binding kinetics of OBS12-18 peptide to the extracellular side of OmpF.
Figure S4. Binding kinetics of the OBS254-63 peptide to the periplasmic side of OmpF.
Figure S5. OBS1 enters OmpF from the periplasmic side with its N terminus first.
Figure S6. OBS2 does not bind in an orientation in which the N terminus points towards the extracellular side.
Figure S7. Current-voltage plots of individual OmpF pores before and after the addition of the IUTD and the IUTD-fusion.
Figure S8. The third OmpF subunit is occluded by the addition of OBS12-26 peptide.
Figure S9. A fusion tag also occludes the third OmpF subunit.
Figure S10. The deletion of either OBS1 or OBS2 perturbs the two-step translocation through OmpF.
Figure S11. Dependence of the translocation of the IUTD-fusion through OmpF on voltage and concentration.
Figure S12. Comparison of kinetic rate constants for OmpF translocation by the untagged IUTD and the IUTD-fusion.
Table S1. Rate constants for the interactions of the IUTD-fusion and the IUTD with OmpF.
Table S2. Rate constants for the interactions of the IUTD-fusion mutants to OmpF.
Table S3. Effective molarities of the IUTD-fusion and the IUTD-fusion mutants.

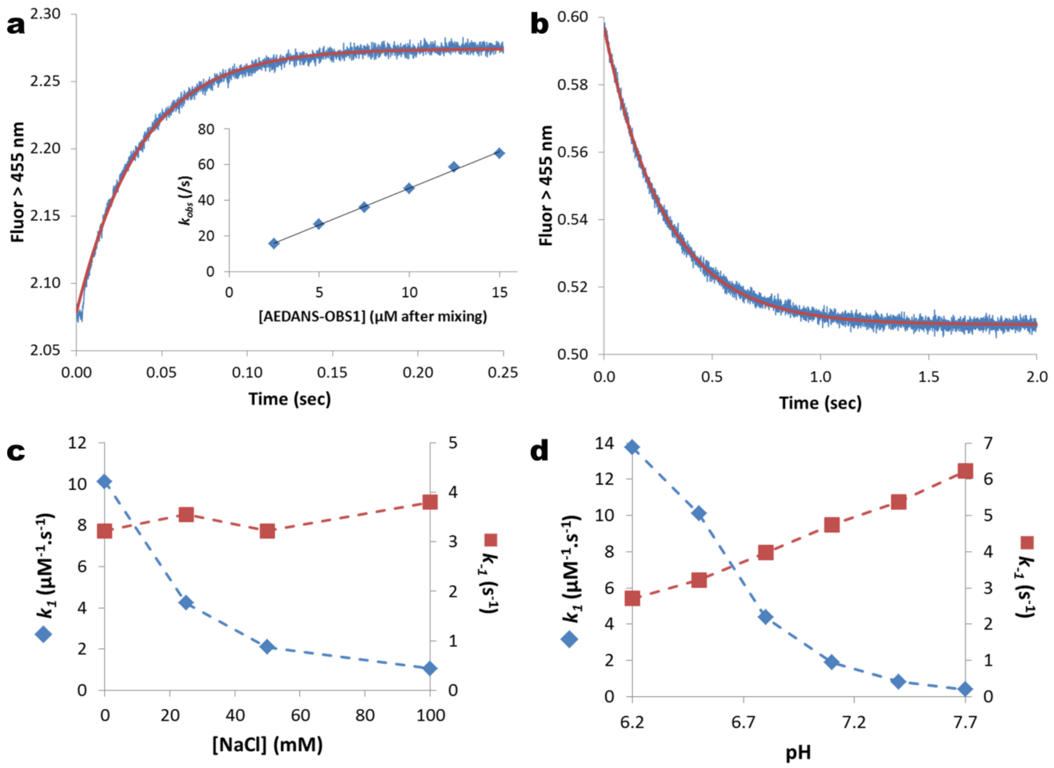

Figure S1. Pre-equilibrium fluorescence measurements for the OmpF–OBS1 complex formation and dissociation at different salt concentrations and pH values. OBS1 in the context of OBS1$_{1\text{-}32}$-E9 DNase·Im9 (T25C) was labelled on the cysteine with IAEDANS (OBS1-AEDANS), allowing FRET between the tryptophans of OmpF (residues 61 and 214) and the AEDANS upon complex formation. Data were collected on an Applied Photophysics SX18 stopped-flow apparatus using an excitation wavelength of 280 nm and fluorescence emissions >455 nm selected with a cut-off filter. **a**, Rise in AEDANS fluorescence upon 5 µM AEDANS-OBS1 binding to 0.165 µM OmpF in 20 mM potassium phosphate, pH 6.5, 25 mM NaCl and 1% (w/v) β-OG, at 10°C. Data were fitted to a single exponential equation to determine k_{obs}, and k_1 was determined from the gradient of k_{obs} plotted against AEDANS-OBS1 concentration (k_1 = 9.80 ± 0.31 µM^{-1}s^{-1}). **b,** Dissociation of the complex formed between 0.33 µM OmpF and 1 µM AEDANS-OBS1 after mixing with 20 µM unlabelled OBS1 peptide. The dissociation rate constant (k_{-1} = 3.22 ± 0.03 s^{-1}) was determined by fitting the data to a single exponential equation. The errors are determined from the deviation of two repeats. **c,** Effect of ionic strength on AEDANS-OBS1 binding OmpF**.** Association and dissociation rate constants were measured in 20 mM potassium phosphate, pH 6.5, 1% (w/v) β-OG, varying NaCl concentration between 0 and 100 mM. The association rate constant decreased with increasing NaCl concentration, whereas the dissociation rate constant remained the same. In comparison with no salt, 100 mM NaCl resulted in a 10-times lower affinity of OBS1 binding to OmpF. **d**, Impact of pH on AEDANS-OBS1 binding to OmpF. Association and dissociation rate constants were measured in 20 mM potassium phosphate, 1% (w/v) β-OG over the pH range of 6.2 to 7.7.

The association rate constant decreased with increasing pH, by up to 80-fold, whereas the dissociation rate constant increased only by a factor of 2.

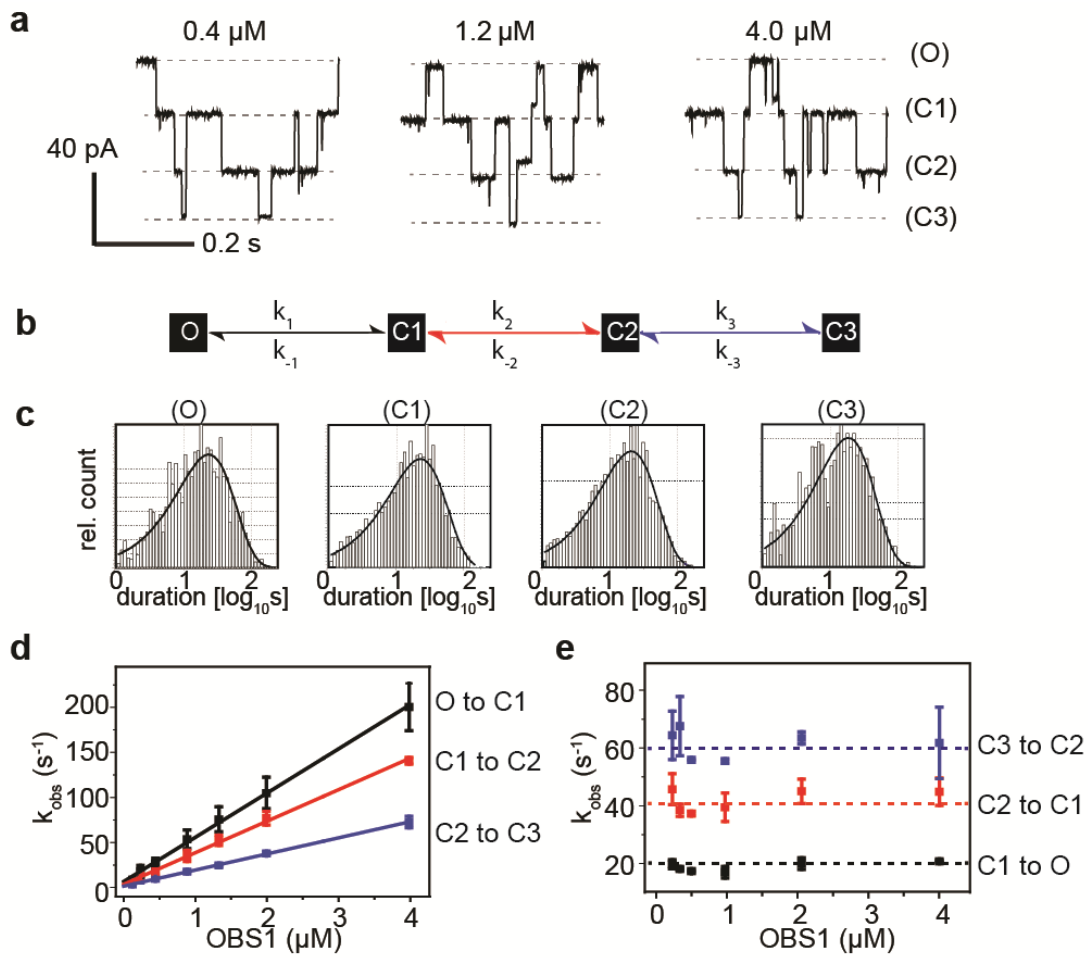

Figure S2. Concentration dependence of OBS1$_{2\text{-}18}$ peptide binding to the periplasmic side of OmpF. a, Current traces of OmpF after 0.4 μM, 1.2 μM, and 4.0 μM OBS1$_{2\text{-}18}$ were added to the periplasmic side of OmpF at an applied potential of +100 mV in phosphate buffer pH 6.4, 100 mM KCl. First, second, and third subunit occlusions were observed in a stepwise manner. **b**, A reaction scheme describing the sequential occlusion of OmpF. **c**, Normalized histograms of dwell-times in each state of OmpF in presence of 0.4 μM OBS1 peptide on the periplasmic side. The data included thousands of binding events. Mean dwell-times and k_{obs} values (for both association and dissociation) were obtained by fitting the histograms to maximum interval likelihood functions by using QuB software. **d**, Concentration dependence of OBS1$_{2\text{-}18}$ association with OmpF. Association rate constants (k_1, k_2, k_3) were determined from the linear dependence of k_{obs} values on OBS1$_{2\text{-}18}$ concentration. **e**, Concentration independent dissociation of OBS1$_{2\text{-}18}$ from OmpF. Dissociation rate constants (k_{-1}, k_{-2}, k_{-3}) were determined by taking average values of k_{obs} over the range of OBS1$_{2\text{-}18}$ concentrations. At least three repeats at each concentration were performed.

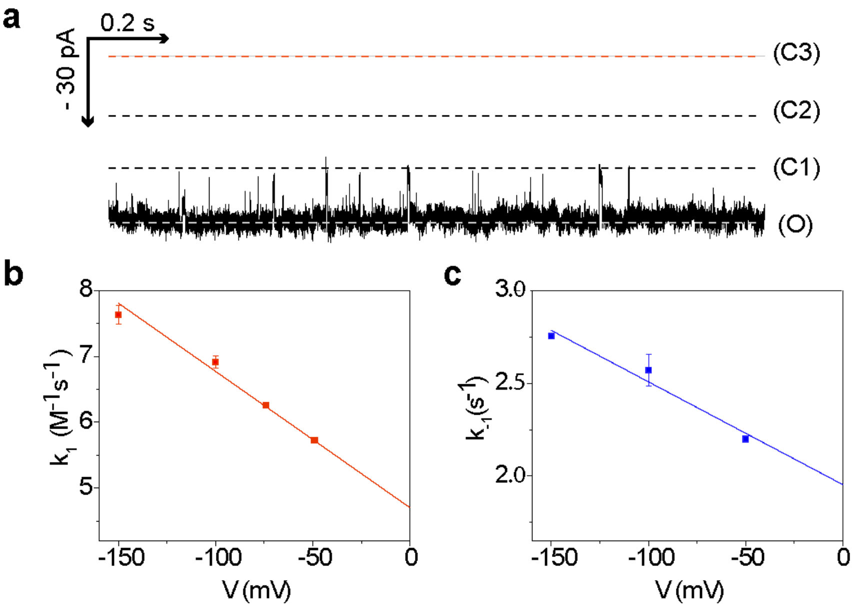

d

k_1 (10^6 $M^{-1}s^{-1}$)	0.050 ± 0.013
k_{-1} (s^{-1})	90 ± 25
K_d (mM)	5.4 ± 2.1

Figure S3. Binding kinetics of OBS1$_{2\text{-}18}$ peptide to the extracellular side of OmpF. a, A representative current trace of OBS1$_{2\text{-}18}$ (8 μM) binding to the extracellular side of OmpF at -100 mV in phosphate buffer pH 6.4, 100 mM KCl. Reversible one-step binding events of OBS1$_{2\text{-}18}$ to OmpF were observed. **b**, A plot of the logarithm of the association rate constant of OBS1$_{2\text{-}18}$ to OmpF from the extracellular side (k_1) versus the applied potential. **c**, A plot of the logarithm of the dissociation rate constant of OBS1$_{2\text{-}18}$ from the extracellular side OmpF (k_{-1}) versus the applied potential. **d**, Table of rate constants at 0 mV estimated by extrapolating the linear dependences shown in (b) and (c). The dissociation constant (K_d) for the monomer was determined, considering the stochastic effect associated with the OmpF trimer, by dividing k_{-1} by one-third of k_1. The data included thousands of binding events. At least two repeats were performed at each concentration and applied potential. Errors are the standard deviations of the repeats.

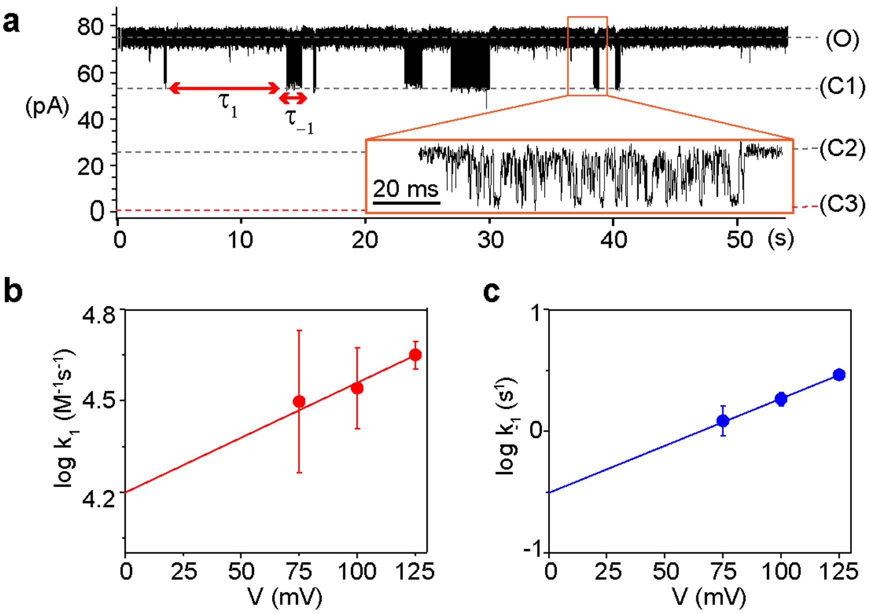

d

k_1 (10^6 $M^{-1}s^{-1}$)	0.015 ± 0.009
k_{-1} (s^{-1})	0.3 ± 0.1
K_d (μM)	60 ± 39

Figure S4. Binding kinetics of the OBS2$_{54\text{-}63}$ peptide to the periplasmic side of OmpF. a, A representative current trace of OBS2$_{54\text{-}63}$ (5 μM) binding to the periplasmic side of OmpF (+100 mV) in phosphate buffer pH 6.4, 100 mM KCl. The binding of OBS2$_{54\text{-}63}$ to OmpF caused subsecond-to-seconds-long clusters of events as shown in the orange box. OBS2$_{54\text{-}63}$ may remain associated with OmpF at the periplasmic entrance after initial binding and unbinding. Thus, we defined dwell times for the unoccupied state and the occupied state as τ_1 and τ_{-1} with a cutoff of 10 ms. Mean dwell-times were determined by using QuB software. **b**, A plot of the logarithm of the association rate constant of OBS2$_{54\text{-}63}$ to OmpF from the periplasmic side (k_1) versus the applied potential. **c**, A plot of the logarithm of the dissociation rate constant of OBS2$_{54\text{-}63}$ from the periplasmic side OmpF (k_{-1}) versus the applied potential. **d**, Table of rate constants at 0 mV estimated by extrapolating the linear dependences shown in (b) and (c). The dissociation constant (K_d) for the monomer was determined from k_1 and k_{-1}, by dividing k_1 by three to remove the stochastic effect associated with the OmpF trimer. The data included hundreds of binding events. At least two repeats were performed at each concentration and applied potential. Errors are the standard deviations of the repeats.

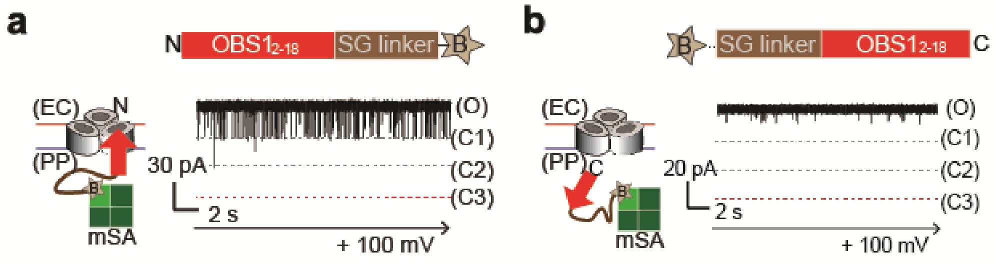

Figure S5. OBS1 enters OmpF from the periplasmic side with its N terminus first. Current traces of OmpF upon the addition of (**a**) the C-terminus capped or (**b**) the N-terminus capped OBS1 sequence to the periplasmic side at an applied potential of +100 mV in phosphate buffer pH 6.4, 100 mM KCl. The C-terminus capped OBS1 and the N-terminus capped OBS1 were prepared by incubating biotinylated OBS1 constructs and monovalent streptavidin (mSA) at a molar ratio of 1:1. Biotinylated OBS1 conjugates contain biotinylated cysteine (grey star) either at the C-terminus (for the C-terminus capped) or at the N-terminus (for the N-terminus capped), separated from the OBS1 sequence by a serine glycine (SG) linker (brown bar). **a**, Upon the addition of the C-terminus capped OBS1-mSA (OBS1-mSA, 2 µM) one-step reversible binding events were observed. This indicates OBS1 can enter from the periplasmic entrance with its N-terminus first. **b**, Upon the addition of the N-terminus capped mSA-OBS1 (mSA-OBS1, 6 µM) current fluctuations occurred only sparsely. This indicates that mSA-OBS1 does not enter OmpF with its C-terminus first. At least three independent experiments were performed in each case.

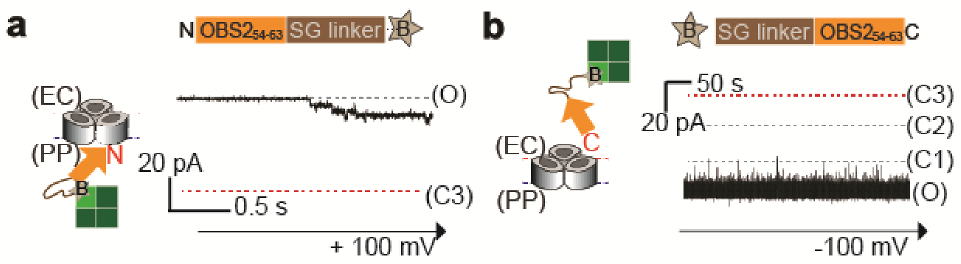

Figure S6. OBS2 does not bind in an orientation in which the N terminus points towards the extracellular side. Current traces of OmpF upon the addition of (**a**) the C-terminus capped OBS2 complex (OBS2-mSA) to the extracellular side and (**b**) the C-terminus capped OBS2 complex (mSA-OBS2) to the periplasmic side in phosphate buffer pH 6.4, 100 mM KCl. The OBS2-mSA and mSA-OBS2 complexes were prepared using the same protocol as described previously (Fig. S5). **a**, The addition of the C-terminus capped OBS2-mSA complex (1 μM) to the periplasmic side at applied potential of +100 mV produced minor current changes, up to 10 pA, which is less than a half the conductance of a single OmpF subunit. Possibly, OBS2 associates with the periplasmic mouth of OmpF but cannot enter the lumen with its N terminus first. **b**, The addition of the N-terminus capped mSA–OBS2 complex (5 μM) to the extracellular side showed hardly any current fluctuations over 10 minutes, indicating that OBS2 does not enter OmpF from the extracellular side with its C terminus first. At least three independent experiments were performed in each case.

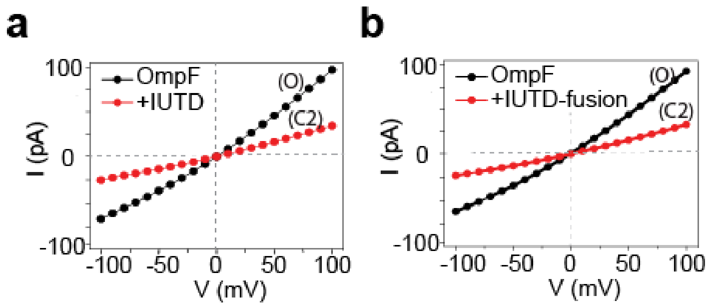

Figure S7. Current-voltage plots of individual OmpF pores before and after the addition of the IUTD and the IUTD-fusion. OmpF shows a positive asymmetric I-V curve with higher conductance at higher potential (*cis*-extracellular, *trans*-periplasmic, black). After the addition to the extracellular side of **a**, untagged IUTD or **b**, the IUTD-fusion, the conductance of OmpF decreased to one-third (C2 state) at both positive and negative applied potentials (red) and the I-V curve remained positive asymmetric.

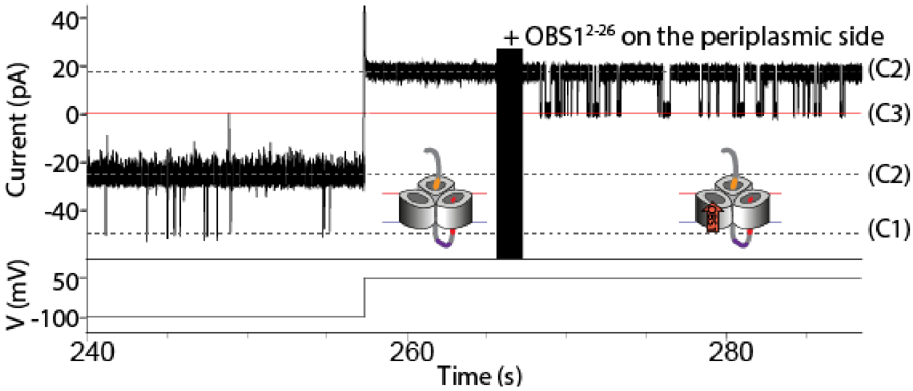

Figure S8. The third OmpF subunit is occluded by the addition of OBS1$_{2-26}$ peptide. The availability of the third OmpF pore was examined after blockade by untagged IUTD followed by the addition of the OBS1$_{2-26}$ peptide to the periplasmic side. Upon the addition of untagged IUTD to the extracellular side, two OmpF subunits were occluded (C2) at an applied potential of -100 mV. To avoid additional events, the remaining IUTD on the extracellular side was removed by repeated buffer exchange. At + 50 mV, 1 µM OBS1$_{2-26}$ peptide was added to the periplasmic side and reversible binding events were observed between current levels C2 and C3. This indicates that the third subunit is available to bind peptide.

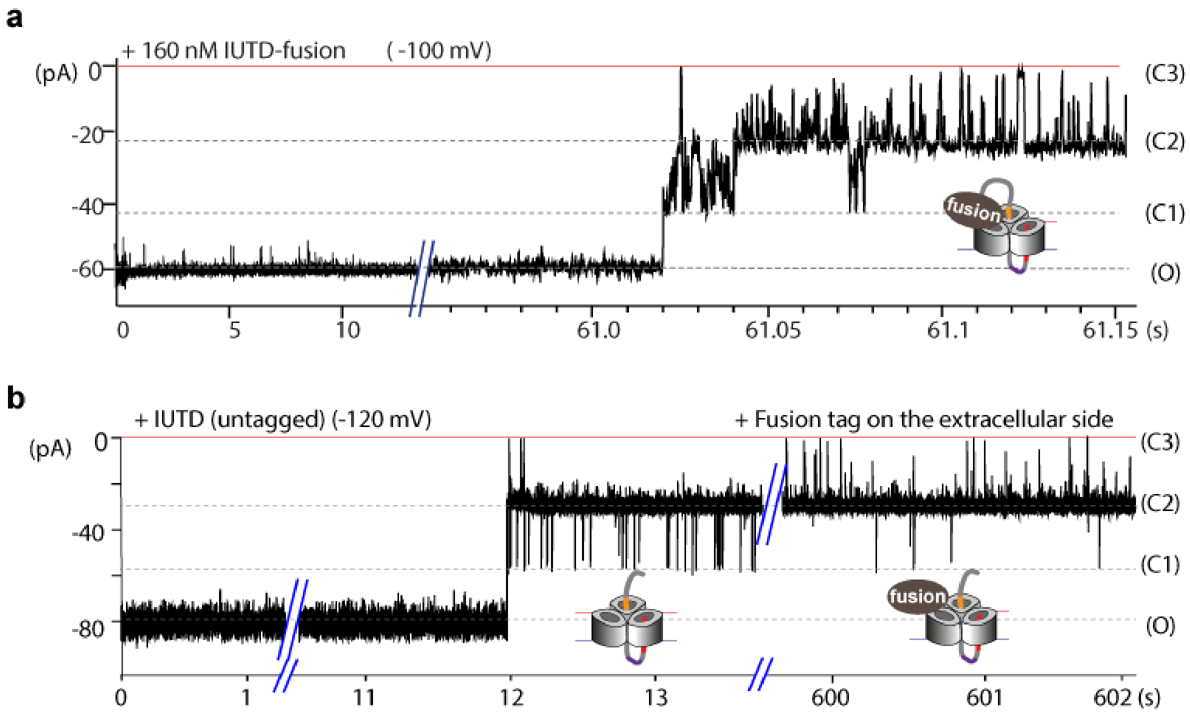

Figure S9. A fusion tag also occludes the third OmpF subunit. a, A current trace of OmpF after the addition of the IUTD-fusion construct (160 nM) to the extracellular side at an applied potential of -100 mV in phosphate buffer pH 6.4, 100 mM KCl. As previously observed with untagged IUTD (Fig. 3b), the conductance was reduced to one-third of the open level (C2) and remained there for most of time. However, the IUTD-fusion construct produced additional fluctuations between levels C2 and C3. **b**, A current trace of OmpF upon the addition of 100 nM untagged IUTD followed by 2 µM fusion-tag only to the extracellular side at an applied potential of -120 mV. After the addition of the fusion-tag, fluctuations between levels C2 and C3 appeared. These data suggest that the transitions between C2 and C3 are produced by the binding of the fusion tag to the extracellular surface of OmpF.

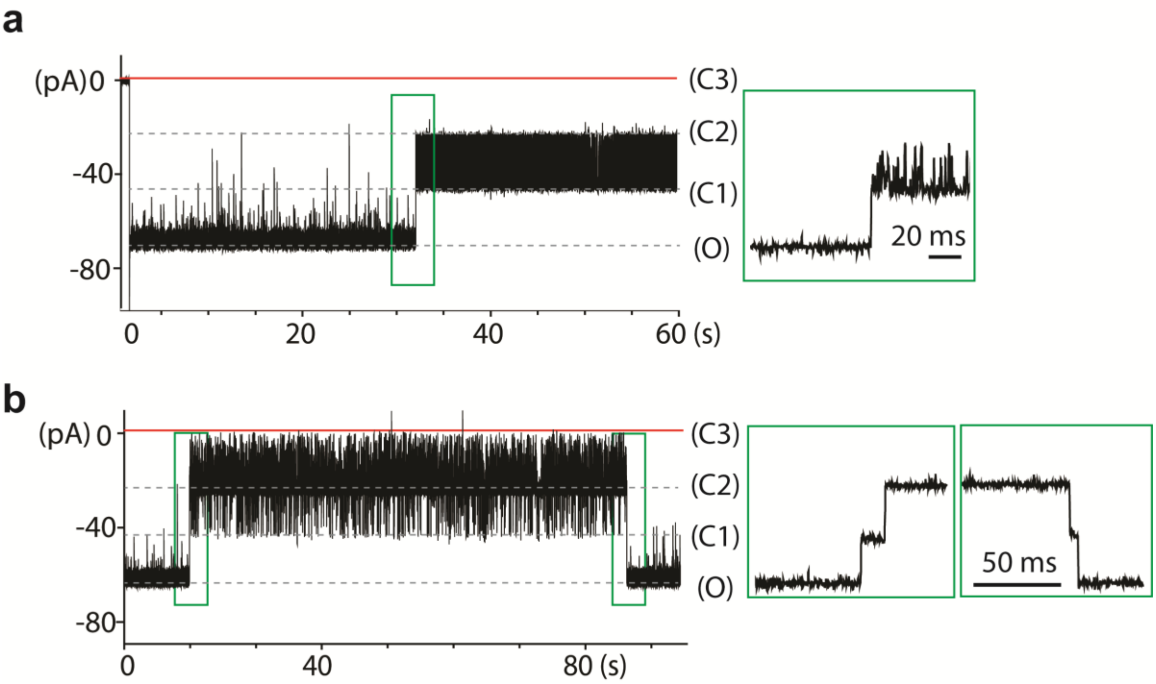

Figure S10. The deletion of either OBS1 or OBS2 perturbs the two-step translocation through OmpF. a, A current trace of OmpF with 1 µM IUTD(ΔOBS1)-fusion, lacking 32 residues at the N terminus, at an applied potential of -100 mV in phosphate buffer pH 6.4, 100 mM KCl. The green box shows a zoomed-in region. Without the OBS1 sequence, only transient binding to the second-subunit was observed. **b**, A current trace of OmpF with 1 µM IUTD(ΔOBS2)-fusion, lacking the $OBS2_{54\text{-}63}$ sequence, under the same conditions as in S10a. The green boxes show zoomed-in regions. The two-step translocation was observed but it was reversed within 1 min. The third subunit occlusion (C3) is induced by the fusion-tag. At least three independent experiments were performed in each case.

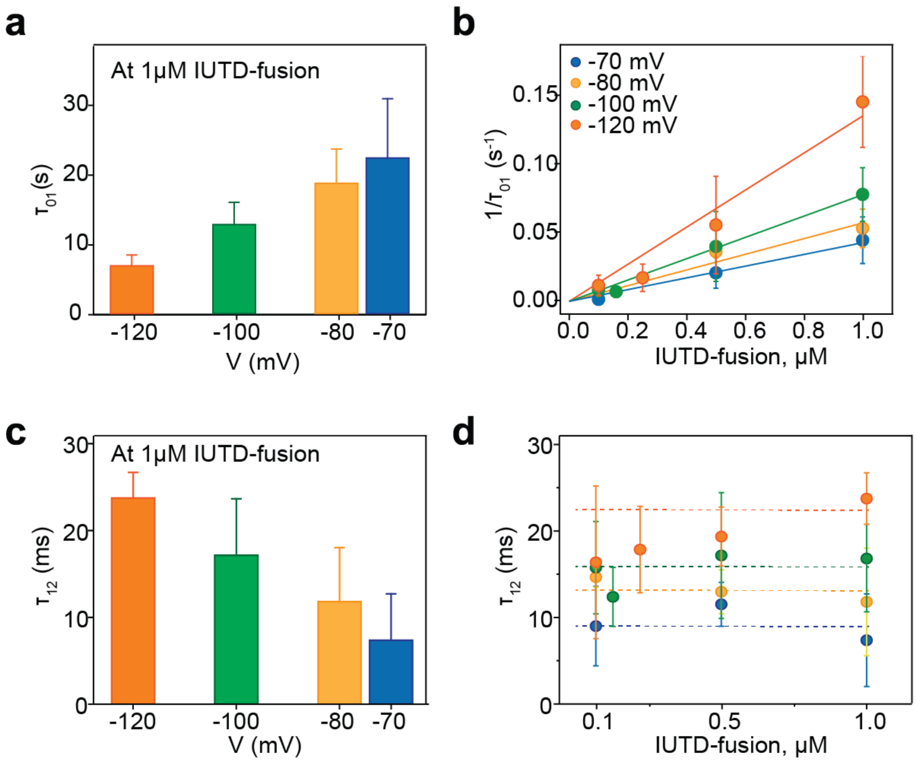

Figure S11. Dependence of the translocation of the IUTD-fusion through OmpF on voltage and concentration. a, A bar chart of mean dwell times before the association of 1 μM IUTD-fusion with OmpF (τ_{01}) at different applied potentials. The values for the mean dwell times (± standard deviation) are 30 ± 6.7 s at -70 mV, 24 ± 6.1 s at -80 mV, 15 ± 2.9 s at -100 mV, and 11 ± 4 s at -120 mV. **b**, The concentration dependence of IUTD-fusion binding to the extracellular side OmpF, plotting the inverse of the mean dwell times (1/ τ_{01}). The association rate constants (k_{01}) at various potentials were determined by fitting the linear gradient to the concentration of the IUTD-fusion: 4.3 ± 0.23 X10^4 $M^{-1}s^{-1}$, 5.7 ± 0.78 X10^4 $M^{-1}s^{-1}$, 7.8 ± 0.28 X10^4 $M^{-1}s^{-1}$, and 14 ± 1.2 X10^4 $M^{-1}s^{-1}$ for -70 mV, -80 mV, -100 mV, and -120 mV, respectively. **c**, A bar chart of mean dwell times (± standard deviation) for the second step in the interaction of 1 μM IUTD-fusion with OmpF (τ_{12}) at different applied potentials. Mean dwell-times are: 7.4 ± 5.4 ms at -70 mV, 12 ± 6.2 ms at -80 mV, 17 ± 6.5 ms at -100 mV, and 24 ± 3.0 ms at -120 mV, respectively. **d**, The concentration independence of the second step. Dashed lines indicate the averages of the mean dwell-times over the various concentrations. The association rate constants (k12) at various potentials were determined by taking the average of 1/ τ_{12}.

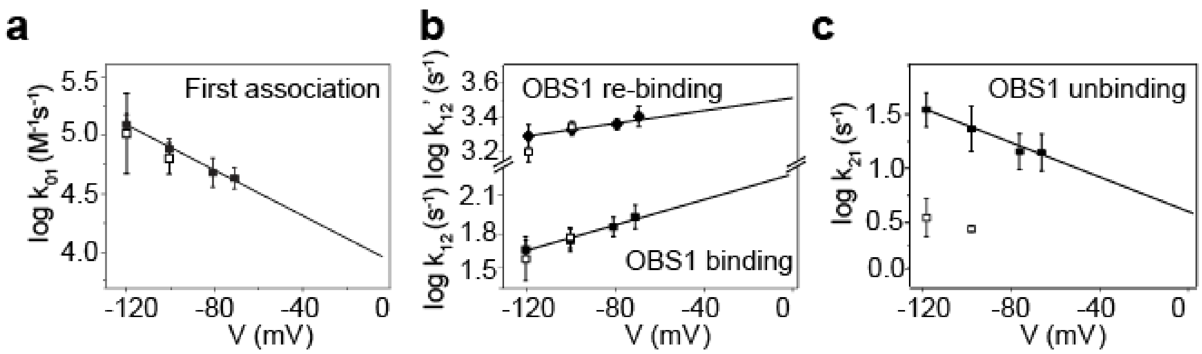

Figure S12. Comparison of kinetic rate constants for OmpF translocation by the untagged IUTD and the IUTD-fusion. a, A plot of the logarithm of association rate constants (k_{01}) versus the applied potential: untagged IUTD (□); IUTD-fusion (●). **b**, A plot of the logarithm of rate constants for binding to the second subunit (initial binding k_{12}, rebinding k_{12}') versus the applied potential. **c**, A plot of the logarithm of rate constants for unbinding from the second subunit of OmpF (k_{21}) versus the applied potential. For k_{01}, k_{12}, and k_{12}', there are no observable differences between untagged IUTD and the IUTD-fusion. For unbinding, there is an about ten-fold difference in k_{21}, probably due to the presence of the fusion-tag.

Table S1. Rate constants for the interactions of the IUTD-fusion and the IUTD with OmpF

	-70 mV	-80 mV	-100 mV	-120 mV
	Association with a first subunit: k_{01} (10^4 $M^{-1}s^{-1}$)			
IUTD-fusion	4.5 ± 0.33	7.5 ± 1.3	9.7 ± 1.1	14 ± 0.65
IUTD*	-	-	6.3 ± 1.9	10 ± 4.1
	Initial binding of the OBS1 sequence to a second subunit: k_{12} (s^{-1})			
IUTD-fusion	80 ± 19	68 ± 13	52 ± 11	44 ± 8.1
IUTD	-	-	58 ± 13	38 ± 17
	Rebinding of the OBS1 sequence to a second subunit: k_{12}' (s^{-1})			
IUTD-fusion	2800 ± 410	2300 ± 190	2000 ± 200	1800 ± 330
IUTD	-	-	2200 ± 270	1400 ± 340
	Unbinding of the OBS1 sequence from the second subunit: k_{21} (s^{-1})			
IUTD-fusion	12 ± 5.2	13 ± 5.3	22 ± 11	35 ± 13
IUTD	-	-	2.6 ± 1.1	3.4 ± 0.7

Rate constants represent the mean value (± s.d.) obtained from at least three and up to twenty independent experiments under the various conditions.

* To initiate translocation of the free IUTD at submicromolar concentrations, we applied higher potentials, -100 mV and -120 mV.

Table S2. Rate constants for the interactions of the IUTD-fusion mutants to OmpF

	- 70 mV	-80 mV	- 100 mV	-120 mV
	Association with a first subunit: k_{01} (10^4 $M^{-1}s^{-1}$)			
IUTD(Δ13)-fusion*	9.2 ± 2.7	-	33 ± 12	-
IUTD(Δ6)-fusion	2.2 ± 0.94	2.4 ± 1.1	3.3 ± 0.8	4.7 ± 3.1
IUTD(12T)-fusion	3.8 ± 0.51	6.3 ± 1.4	13 ± 5.2	30 ± 5.1
IUTD(T6)-fusion	3.6 ± 0.85	3.5 ± 2.2	4.9 ± 1.7	7.5 ± 2.0
	Initial binding of the OBS1 sequence to a second subunit: k_{12} (s^{-1})			
IUTD(Δ13)-fusion	5.5 ± 3.8	-	3.0 ± 0.7	-
IUTD(Δ6)-fusion	24 ± 4.7	18 ± 2.6	17 ± 4.4	13 ± 8.1
IUTD(12T)-fusion	100 ± 59	98 ± 18	71 ± 33	70 ± 9.0
IUTD(T6)-fusion	51 ± 9.6	46 ± 15	38 ± 13	32 ± 6.7
	Rebinding of the OBS1 sequence to a second subunit: k_{12}' (s^{-1})			
IUTD(Δ6)-fusion	2100 ± 310	2100 ± 100	1800 ± 280	1500 ± 310
IUTD(12T)-fusion	1700 ± 510	1600 ± 80	1400 ± 140	1300 ± 90
IUTD(T6)-fusion	2600 ± 330	1900 ± 440	1400 ± 40	870 ± 70
	Unbinding of the OBS1 sequence from the second subunit: k_{21} (s^{-1})			
IUTD(Δ6)-fusion	16 ± 10	8.9 ± 1.6	27 ± 13	39 ± 2.4
IUTD(12T)-fusion	0.4 ± 0.16	5.3 ± 1.3	5.3 ± 1.9	1.7-± 0.6
IUTD(T6)-fusion	2.6 ± 0.3	1.9 ± 0.6	5.1 ± 1.4	6.9 ± 0.58

Rate constants are the mean value (± s.d.) obtained from at least three independent experiments under the various conditions.

* The IUTD(Δ13)-fusion showed few transitions between C1 and C2. Therefore, only the rate constants for the initial associations (k_{01} and k_{12}) are given here.

Table S3. Effective molarities of the IUTD-fusion and the IUTD-fusion mutants

	EM^1 (mM)	EM^2 (mM)
IUTD-fusion	0.030 ± 0.006	0.91 ± 0.26
IUTD(Δ6)-fusion	0.008 ± 0.003	0.58 ± 0.16
IUTD(12T)-fusion	0.031 ± 0.013	0.31 ± 0.02
IUTD(T6)-fusion	0.019 ± 0.006	0.31 ± 0.02

The effective molarities (EM) were determined from the ratio of the rate of binding of the OBS1 segment in the fusion construct to OmpF to the rate constant for the bimolecular binding of the $OBS1_{2-18}$ peptide. EM_1 and EM_2 are effective molarities for the initial binding of the OBS1 segment to OmpF (k_{12}) and for the re-binding (k_{12}'), respectively. Rate constants extrapolated to 0 mV were used.